ULTRASTABLE LONG-DISTANCE FREQUENCY DISSEMINATION THROUGH OPTICAL FIBRES

A Degree Thesis

Submitted to the Faculty of the

Escola Tècnica d'Enginyeria de Telecomunicació de Barcelona

Universitat Politècnica de Catalunya

by

Clàudia de la Monja Rico

In partial fulfilment

of the requirements for the degree in

TELECOMMUNICATIONS ENGINEERING

Advisor: María Santos Blanco

Barcelona, June 2022

Abstract

Nowadays, a large number of applications require highly stable frequency dissemination, such as deep space networks for interferometric imaging with arrays formed by antennas located very far apart. To accomplish this demand for stability, optical fibre links are used due to the advantages of low cost, low attenuation, and immunity to electromagnetic interference.

The system studied in this thesis guarantees a high precision among the signals of all the antennas in an array by connecting them coherently in a fibre ring architecture. Through recirculation of a phase conjugated signal, the compensation of the phase instability generated in long distance fibre links by temperature changes and vibrations of the environment is achieved. Nevertheless, the non-idealities of the system's components may add a random effect in this phase compensation that is analysed using the Allan deviation as a metric factor, with the aim to establish the loss in stability of the frequency dissemination system.

Resum

Actualment, un gran nombre d'aplicacions requereixen d'una alta estabilitat en la propagació de freqüència, com les xarxes de l'espai profund per la interferometria d'imatge del cel amb agrupacions d'antenes molt allunyades geogràficament. Per satisfer aquesta demanda d'estabilitat, s'utilitzen enllaços de fibra òptica degut a avantatges com el seu baix preu, baixa atenuació i immunitat a la interferència electromagnètica.

El sistema que s'estudia en aquesta tesi garanteix una alta precisió entre les senyals de totes les antenes d'una agrupació, connectant-les coherentment en una arquitectura d'anell de fibra. Per mitjà de la recirculació d'una senyal conjugada en fase, s'aconsegueix la compensació de la inestabilitat de fase que es genera als enllaços de fibra llargs pels canvis de temperatura i les vibracions del medi. Tanmateix, les no idealitats dels components del sistema poden afegir un efecte aleatori a aquesta compensació de fase, que és analitzat utilitzant la desviació d'Allan com a paràmetre de mesura amb l'objectiu de determinar les pèrdues en l'estabilitat del sistema de propagació de freqüència.

Resumen

Actualmente, un gran número de aplicaciones requieren de una alta estabilidad en la propagación de frecuencia, como las redes del espacio profundo para la interferometría de imagen del cielo con agrupaciones de antenas muy separadas geográficamente. Para satisfacer esta demanda de estabilidad, se usan enlaces de fibra óptica debido a sus ventajas como el bajo precio, baja atenuación e inmunidad a la interferencia electromagnética.

El sistema que se estudia en esta tesis garantiza una alta precisión entre las señales de todas las antenas de una agrupación, conectándolas de manera coherente en una arquitectura de anillo de fibra. Por medio de la recirculación de una señal conjugada en fase, se consigue la compensación de la inestabilidad de fase que se genera en los enlaces de fibra largos por los cambios de temperatura y las vibraciones del medio. Sin embargo, las no idealidades de los componentes del sistema pueden añadir un efecto aleatorio a esta compensación de fase, que se analiza usando la desviación de Allan como parámetro de medida con el objetivo de determinar las pérdidas en la estabilidad del sistema de propagación de frecuencia.

This thesis is dedicated to my parents, who always believed in me, and to Marc, my everyday support.

Acknowledgements

I would like to thank my supervisor, María Santos, for trusting me and encouraging me to start this project, always providing me the guidance I needed in order to conclude it.

Revision history and approval record

Revision	Date	Purpose
0	08/03/2022	Document creation
1	14/04/2022	Document revision
2	18/06/2022	Document revision

DOCUMENT DISTRIBUTION LIST

Name	e-mail
Clàudia de la Monja Rico	claudia.de.la.monja@estudiantat.upc.edu
María Santos Blanco	m.santos@upc.edu

Written by:		Reviewed and approved by:	
Date	08/03/2022	Date	18/06/2022
Name	Clàudia de la Monja Rico	Name	María Santos Blanco
Position	Project Author	Position	Project Supervisor

Table of contents

List of figures

List of tables

1.   Introduction

The main purpose of this thesis is to unveil the potential of optical fibres for ultrastable radio frequency transport in long distance distributed antennas, analysing a solution based on the passive phase conjugation of a round-trip reference signal achieved by the smart biasing of the push-pull Mach-Zehnder modulators (MZMs) used for optical upconversion, in other words, for the translation of the radiofrequency signals to the optical domain.

The phase conjugation of the reference signal will lead to its phase stabilisation by a passive phase compensation, which allows to have a stabilised signal going through the link of antennas.

The context in which this technology will be applied is high-resolution interferometric imaging in deep space networks. This kind of networks use radio telescopes that require very large antennas to collect enough radio energy from the space and to assure a good angular resolution. To enable these specifications, several radio telescopes separated long distances are coherently connected among them simulating a single one with dimensions equivalent to the separation distances.

To achieve an accurate reconstruction from the signals coming from every telescope, a high precision in their phase information will be crucial. The proposed system interconnects the radio telescopes in a fibre-ring architecture with a central station as the example shown in Figure 1:
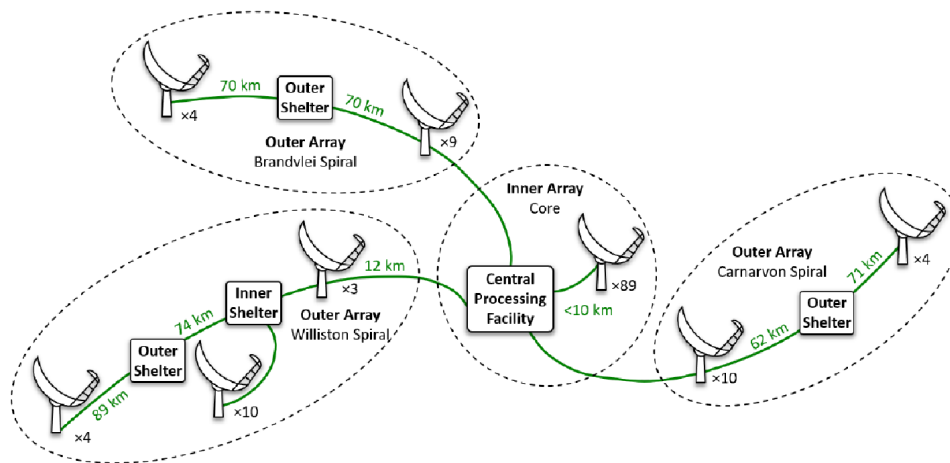
Figure 1: Example of a kilometre array phase synchronisation system

The aforementioned reference stabilised signal is sent from the central station through the link to all of the radio telescopes, operating as a clock to the incoming signals and leading to the knowledge of their phase information.

Once the system and its operating principles have been analysed, the impact of the non-ideal behaviour of its components is characterised using the Allan deviation as a

metric factor as a function of the system's sources of non-linearities, focusing on the MZMs modulation index and extinction ratio (ER).

Fast cancellation of fibre length fluctuations due to environmental factors still remains a challenge, as the most used techniques require highly complex systems and careful adjustment. The main motivation behind this project is to inquire into the potential of optical fibre and photonic components employment in stable long-distance transmission applications by combining RF and photonic techniques, making use of photonic components already present in the system which are needed for the up and downconversion required for the fibre propagation.

2.   State of the art of the technology used or applied in this thesis

Traditional RF applications are expected to progress towards microwave photonics techniques, based on the smart combination of RF and photonic components [1].

One representative case of this growth would be the leadership of optical fibre communications in the ultra-stable long-distance signal transport, demanded in numerous applications related to geodesy, gravitational-wave detection, high-energy accelerators, radio astronomy and global positioning systems, which employ synthetic aperture radar and very-long-baseline interferometers [2] [3] [4].

This thesis aims to dig into this research that mixes radio-frequency (RF) engineering and photo-electronics by studying the ultra-stability potential of large fibre links, focusing on the passive phase conjugation by the frequency mixing of a round-trip signal. This technique is the most promising approach due to its significant advantages over active compensation techniques in terms of lower complexity and higher speed and range [5].

There are several demonstrations of stable frequency dissemination in optical fibres, such as a 150 Km unamplified real world urban fibre network system [6]. Nevertheless, most of these applications use pure-RF implementations that make use of electrical mixers, frequency multipliers/dividers and additional microwave sources, which add complexity and give rise to undesirable spurious [7] [8]. Therefore, more optimal solutions should leverage synergies with photonic components already present in the system for the required optical up and downconversion required for the fibre propagation.

A recent all-optical fibre dissemination scheme has shown good performance over a 20 Km link [9], which is based on exploiting the nonlinear response of the Mach-Zehnder modulator to achieve frequency mixing using different biasing conditions. This is a promising technique, although a lack of quality measure makes it difficult to implement.

The main motivation of this thesis comes from the need to establish a reliable quality measure in this type of microwave photonics techniques, to allow the comparison of the performance between different systems, mainly affected by the quality and state of the integrated components.

3.   Previous concepts

In this chapter, several concepts are explained with the aim to aid the comprehension of the following chapters.

On one hand, it could be said that MZM is the key component of the studied system and that has a certain complexity, so it is important to dig deep into its fundamentals to be able to understand the system's behaviour, and consequently, the instability added mostly by its non-idealities.

On the other hand, the Allan deviation is going to be the parameter used to measure the non-ideal results of the phase compensation, which will be essential in this project.

3.1.   Mach-Zehnder Modulator

The Mach-Zehnder modulator (MZM) is an interferometer, i.e. a device that bases its operation on the phenomenon of interference between waves.

In an interferometer, the input optical signal is divided into two equal parts, each one of them is made to take a different optical path (through one of the two branches of the interferometer, which may have different optical lengths), to be recombined afterwards. When there is no phase difference between both optical paths, the signals along each branch will be recombined constructively at the output of the interferometer, however, when the phase difference is π radians, the signals will interfere destructively at the output.

In a MZM, a voltage is applied to the two branches of the interferometer, altering their relative refractive index and so also their relative optical lengths [10]. Therefore, by modulating the applied voltage the optical signal can be modulated.

Figure 2 represents the structure of the MZM:
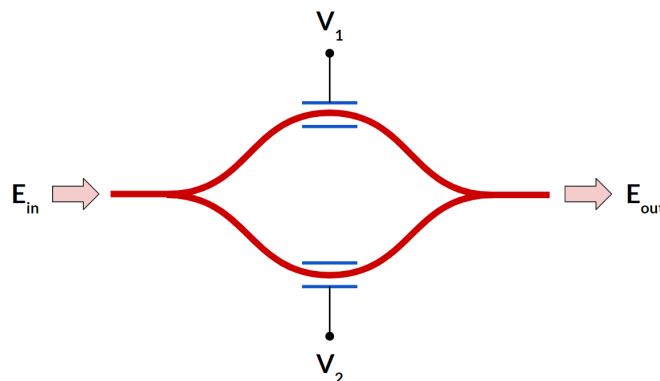
Figure 2: Mach-Zehnder modulator structure

in which electrical signals V_1 and V_2 are the phase shifter's drivers of each branch of the interferometer. When both arms signals are recombined, the resulting optical modulated field is:

$$E_{out} = \frac{E_{in}}{2} \left(e^{j\frac{\pi V_1}{2V_\pi}} + e^{j\frac{\pi V_2}{2V_\pi}} \right) \quad (3.1.1)$$

In a typical push-pull configuration of the MZM, the applied voltages have opposite phase [11]:

$$V_1 = -V_2 \quad (3.1.2)$$

which leads to:

$$E_{out} = \frac{E_{in}}{2} \left(e^{j\frac{\pi V_1}{2V_\pi}} + e^{j\frac{-\pi V_1}{2V_\pi}} \right) = E_{in} \, cos \left(\frac{\pi V}{2V_\pi} \right) \quad (3.1.3)$$

where V_π is a parameter of the MZM named the halfwave voltage, and is defined as the difference between the applied voltage at which the signals in each branch are in phase, and the applied voltage at which the signals are at π radians out of phase [10].

Following, knowing that the power is obtained squaring the electrical field [12]:

$$P_{\text{out}} = P_{in} \cos^2 \left(\frac{\pi V}{2V_\pi} \right) = \frac{P_{in}}{2} \left(1 + \cos \left(\frac{\pi V}{V_\pi} \right) \right) \quad (3.1.4)$$

From equations (3.1.3) and (3.1.4), the transfer functions of a MZM working in push-pull configuration will follow a cosine shape as seen in Figure 3. As can be seen in the mentioned figure, when a MZM operates at the quadrature point (QP) is operating with $V_B = \frac{V_\pi}{2}$, and when it operates at the null point (NP), $V_B = V_\pi$ [12].

The MATLAB code made for Figure 3 representation can be found in Appendix 1.
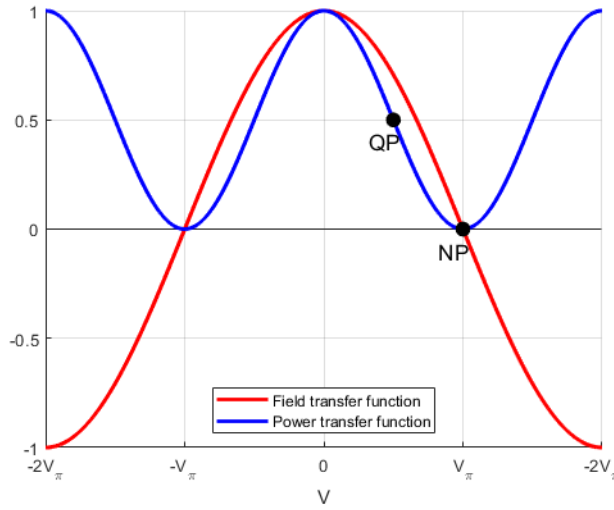
Figure 3: Field and power transfer functions of a Mach-Zehnder modulator in push-pull configuration, with operation point for quadrature point (QP) and for null point (NP)

To follow, the relation between MZM input and output fields is going to be analysed when it is in push-pull configuration.

First, the input voltage V may be expressed as:

$$V = V_B + v_{RF}(t) = V_B + V_{RF} \cos\left(\omega_{RF}t\right) \tag{3.1.5}$$

where V_B corresponds to the bias voltage and $v_{RF}(t)$ to the RF component of the input voltage.

Then, equation (3.1.3) results:

$$E_{\text{out}} = E_{in} \cos\left(\frac{\theta_B + \theta_{RF}(t)}{2}\right) \tag{3.1.6}$$

where θ_B is expressed as:

$$\theta_B = \frac{\pi\, V_B}{V_\pi} \tag{3.1.7}$$

and $\theta_{RF}(t)$ as:

$$\theta_{RF}(t) = \frac{\pi\, v_{RF}(t)}{V_\pi} \tag{3.1.8}$$

Applying to equation (3.1.6) the cosine sum trigonometric identity results:

16

$$E_{out} = E_{in} \left(\cos\left(\frac{\theta_B}{2}\right) \cos\left(\frac{\theta_{RF}(t)}{2}\right) - \sin\left(\frac{\theta_B}{2}\right) \sin\left(\frac{\theta_{RF}(t)}{2}\right) \right) \quad (3.1.9)$$

Then, [13] from equation (3.1.8) and introducing the modulation index m as:

$$m = \frac{\pi V_{RF}}{V_\pi} \quad (3.1.10)$$

Jacobi-Anger expansion can be applied to equation (3.1.9) using $cos(\frac{m}{2}cos(\omega_{RF}t))$ and $sin(\frac{m}{2}cos(\omega_{RF}t))$ as [14]:

$$E_{out} = E_{in} \left(\cos\left(\frac{\theta_B}{2}\right) \left(J_0\left(\frac{m}{2}\right) + 2\sum_{n=1}^{\infty}(-1)^n J_{2n}\left(\frac{m}{2}\right) \cos\left(2n\omega_{RF}t\right) \right) + \right.$$

$$\left. + 2\sin\left(\frac{\theta_B}{2}\right) \sum_{n=1}^{\infty}(-1)^n J_{2n-1}\left(\frac{m}{2}\right) \cos\left((2n-1)\omega_{RF}t\right) \right) \quad (3.1.11)$$

where $J_n(x)$ are the Bessel functions of the first kind [15].

Then, the analysis depends on if the MZM operates in NP or QP:

- For **NP operation**, $V_B = V_\pi$, so $\theta_B = \pi$ and the equation (3.1.11) results:

$$E_{out} = E_{in} \, 2\sum_{n=1}^{\infty}(-1)^n J_{2n-1}\left(\frac{m}{2}\right) \cos\left((2n-1)\omega_{RF}t\right) \quad (3.1.12)$$

As seen in (3.1.12), NP operation gives only the odd harmonics of the RF signal, and suppresses the zeroth and even harmonics [16]. In that point, if m is considered under small-signal assumption $m << 1$ since V_{RF} is much smaller than the halfwave voltage V_π, then only the first and the third harmonics may be considered [17] (in Appendix 2, Bessel functions of the first kind are plotted and may visually facilitate the comprehension of this approximation).

After filtering the first harmonic (which, in power over frequency, has the largest optical output sidebands tones compared to the 3th harmonic tones), a linear electro-optical transfer function may be ensured with this biasing, resulting:

$$E_{out} \approx E_{in} \ cos(\omega_{RF}t)$$

(3.1.13)

- For **QP operation**, $V_B = \frac{V_\pi}{2}$, so $\theta_B = \frac{\pi}{2}$ and then, from (3.1.11), all harmonics of the RF signal are obtained. Under small-signal approximation, only the zero$_{th}$ and the first harmonics may be considered, leading from equation (3.1.11) to:

$$E_{out} \approx E_{in} \left(1 + m \ cos(\omega_{RF}t)\right)$$

(3.1.14)

3.2.   Allan variance

The Allan variance (AVAR, $\sigma_y^2(\tau)$), is a unitless measure of time domain frequency stability, typically used to quantify the stability of clocks and other oscillators [18]. The Allan deviation (ADEV), is the square root of Allan variance.

The AVAR is defined [19] as follows:

$$\sigma_y^2(\tau) = \frac{1}{2} \left\langle (\bar{y}_{k+1} - \bar{y}_k)^2 \right\rangle$$

(3.2.1)

where $\langle \ \rangle$ refers to the expected value, and $\bar{y}_k$ corresponds to the kth average fractional frequency measured over the observation time τ, and is defined as [18]:

$$\bar{y}_k = \frac{1}{n} \sum_{i=k}^{k+n-1} y_i$$

(3.2.2)

where y_i is the fractional frequency corresponding to the ith sample of the data set, with separation between samples τ_0, and the following relation with the observation time τ:

$$\tau = n\tau_0$$

(3.2.3)

If τ_0 is the minimum data spacing for the original stored data set y_k, then one can change the sampling time [18] from τ_0 to τ by averaging n adjacent values of y_k to obtain a new

fractional frequency estimate $\bar{y}_k$ with sample time τ as input to (3.2.1). The reason behind this proceeding is justified in subsection 3.2.1.

Fractional frequency values y_k are the measures of the fractional frequency data set, separated the sample time τ_0 (minimum separation between values). The fractional frequency corresponds to the normalised difference between the frequency of the signal ν_k and the nominal frequency ν_{nom} [20]:

$$y_k = \frac{\nu_k - \nu_{nom}}{\nu_{nom}} \tag{3.2.4}$$

The AVAR definition (3.2.1), is based on the statistical expected value that is the integration over infinite time, which is not allowed in practice because data sets have a finite number of samples. Therefore, the employment of a statistical estimator using M samples of frequency in the available data set will be needed in place of the statistical expected value.

There are several estimators that may be used to compute the AVAR, depending on whether the observation time τ in which the measures of y_k are averaged is fixed or not, as explained below.

- In the **fixed τ case**, $n = 1$, which leads to:

$$\tau = \tau_0 \tag{3.2.5}$$

and, therefore, $\bar{y}_k$ values equals to y_k values as can be seen in (3.2.2) because the averaging time equals to the sample time, where there is only one measurement of y_k to average.

In this case, the estimator will be calculated by directly translating the definition (3.2.1) into:

$$\sigma_y^2(\tau_0, M) = \text{AVAR}(\tau_0, M) = \frac{1}{2(M-1)} \sum_{i=1}^{M-1} \left(\bar{y}_{i+1} - \bar{y}_i \right)^2 \tag{3.2.6}$$

where M is the number of measures in the fractional frequency data set.

In the case of this estimator, the average time (referred also as time of observation) τ is equal to the minimum spacing time between measurements τ_0 thus, as mentioned, $\bar{y}_i = y_i$.

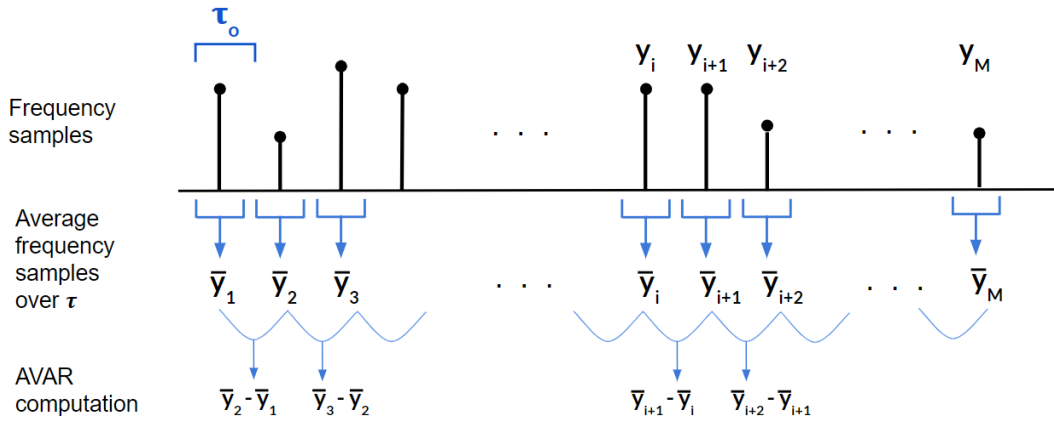Figure 4 introduces a visual scheme of the AVAR calculation with fixed τ estimator:

Figure 4: Scheme of the Allan variance calculation through the fixed τ estimator

As Figure 4 shows, having M frequency measurements each τ_0, M values of average frequency will be created (averaging the frequency values over τ_0). Then, the AVAR will be computed over the resulting values data set.

- In the **variable τ case**, $n \neq 1$ and τ results as introduced above in the general case in (3.2.3).

In this case, the estimators can be computed in an "overlapped" or "non-overlapped" way, as explained below:

- The **non-overlapped** variable τ estimator, calculated as:

$$\sigma_y^2\left(n\tau_0, M\right) = \mathrm{AVAR}\left(n\tau_0, M\right) = \frac{1}{2\frac{M-1}{n}} \sum_{i=1}^{\frac{M-1}{n}} \left(\bar{y}_{ni+n} - \bar{y}_{ni}\right)^2 \qquad (3.2.7)$$

where n is the integer number multiplying τ_0.

Figure 5 is a scheme of how this estimator is calculated, in the case of $n = 3$. As can be seen in the figure, Having M frequency measurements each τ_0, $M - n + 1$ frequency averages will be extracted by averaging the M frequency values in windows of $n = 3$ measures, each window separated τ_0 from the previous one. This can be seen as obtaining n additional data sets (blue, green, and orange in this example) out of the original data set, each of them with a new sample time τ. Then, only the resulting average measures pertaining to the new data set formed over the first frequency measure ($\bar{y}_1$, $\bar{y}_{1+n}$, $\bar{y}_{1+2n}$...) will be used to calculate the AVAR.
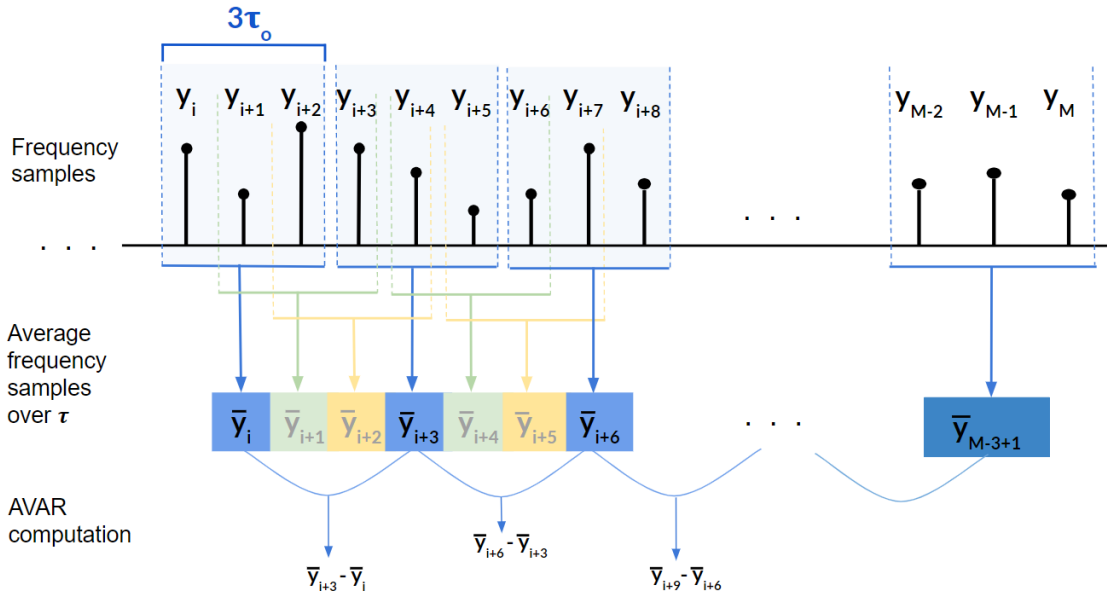
Figure 5: Scheme of the calculation of the Allan variance through the non-overlapped variable τ estimator, assuming $\tau = 3\tau_0$

Something to be aware of is that the measurements of $\bar{y}_k$ used to calculate the estimator are separated by n samples in the resulting average fractional frequency data set, but actually pertaining to adjacent measures of observation time τ, which may be seen as a new sample time. Ultimately, $\bar{y}_{ni+n}$ and $\bar{y}_{ni}$ in the estimator calculation pertain to adjacent clusters taking into account the new sample time, because there is no dead time between the measurements.

It is proper to also notice that, with this estimator, only $\frac{1}{n}$ of the available samples of $\bar{y}_k$ are used, which is a significant drawback.

- The **overlapped** variable τ estimator, calculated as [21]:

$$\sigma_y^2(n\tau_0, M) = \frac{1}{2(M - 2n + 1)} \sum_{i=1}^{M-2n+1} (\bar{y}_{i+n} - \bar{y}_i)^2 \qquad (3.2.8)$$

Figure 6 is a scheme of how this estimator is calculated, in the case of $n = 3$:
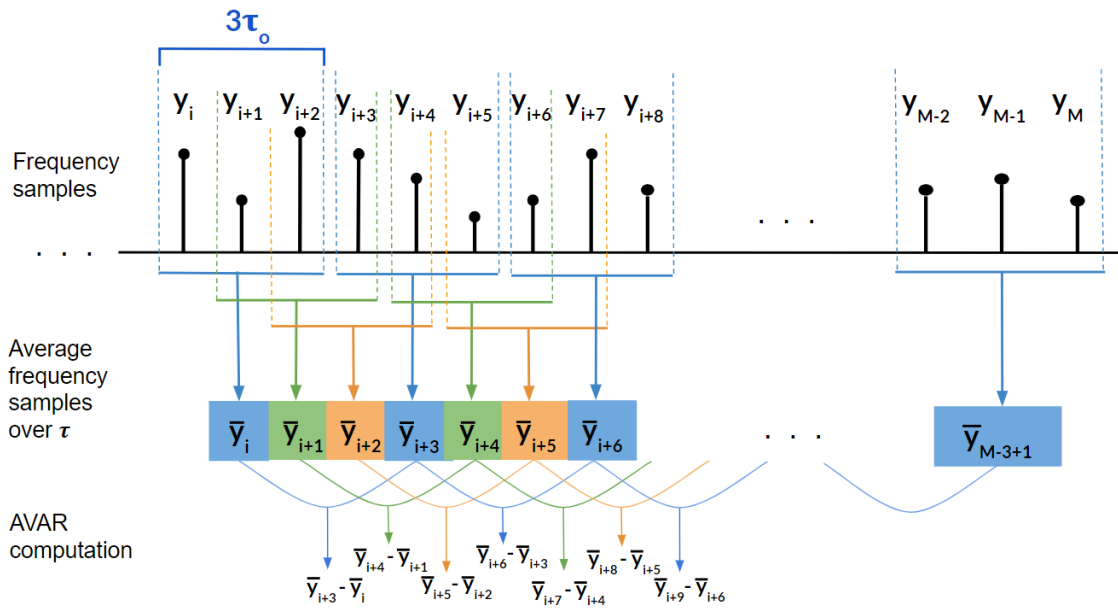
Figure 6: Scheme of the calculation of the Allan variation through the overlapped variable τ estimator, assuming $\tau = 3\tau_0$

As seen in the figure, It follows the same procedure to obtain the average frequency values than in the non-overlapped case (Figure 2), however, in this estimator, all resulting values of average frequency are used to calculate the AVAR, using the n new data sets although they are overlapped in time.

Furthermore, in the computation of the overlapped estimator, n additional terms for each term of the non-overlapped estimator are generated. This leads to a far superior performance over non-overlapped or fixed τ estimators, which makes the overlapped estimator the preferred estimator to calculate the Allan variance [22].

3.2.1. Interpretation of the value

To help understand the meaning of the resulting value, the specific case of a tested clock is a proper example. If the clock under test is compared with a highly more accurate clock (a reference clock), during an interval of time τ measured by the reference clock, the tested clock advances by τy, where y is the tested clock average frequency over that interval. This situation is visually exemplified in Figure 7.

If a consecutive interval is measured and results $\tau y'$, the value of $(y - y')^2$ can be extracted. A smaller value will mean a more stable clock. Then, repeating this procedure many times and averaging the results, twice the Allan variance (or Allan deviation squared) will be obtained.

If these results are calculated for different intervals of time τ, various types of noise sources can be distinguished, and that is why the ADEV is typically represented as a function of τ. Furthermore, different devices could be compared in terms of the level of offered stability.
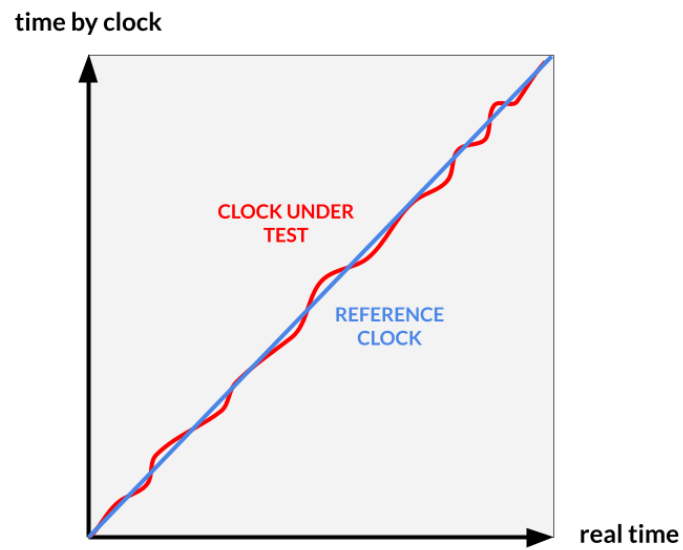
Figure 7: Time readings of a highly precise clock and a tested clock over the real time

In Figure 7, while the reference clock time reading advances in a linear way with real time progression, the clock under test varies its frequency with time, leading to a difference between time reading and actual time.

4.   Project development

After the essential concepts of this thesis development have been introduced in the last chapter, it is already feasible to properly introduce the phase compensation system based on the phase conjugation technique, as well as its main sources of nonlinearities and the acquired method to rate them.

4.1.   Operation principle

The phase compensation method proposed in this thesis provides the phase stabilisation of a radio frequency (RF) reference signal propagating from a central site (CS) to a remote site (RS) located very far apart, as shown in Figure 1, accomplished by the passive phase conjugation of the signal by the utilisation of carefully biassed MZMs in a system whose schematic diagram is shown in Figure 8 [9]:
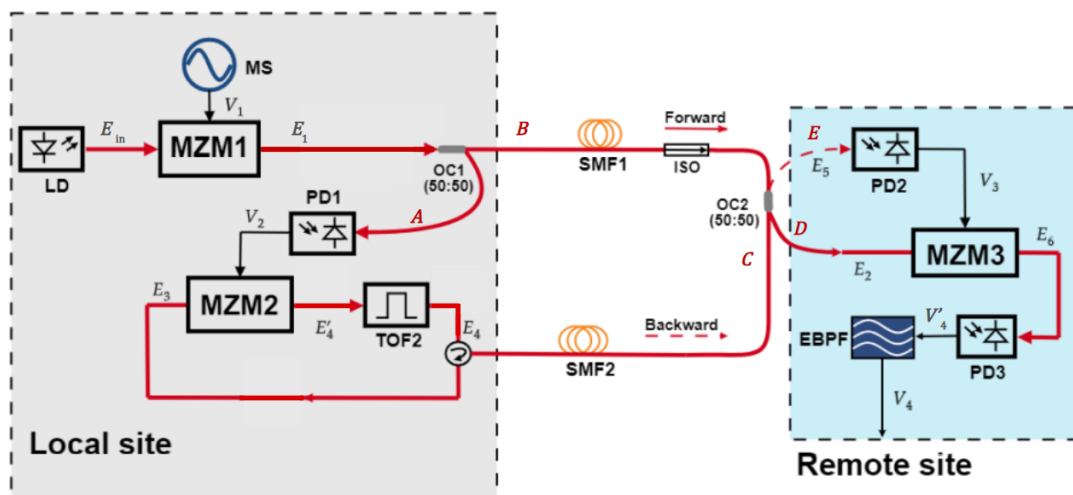
Figure 8: Schematic diagram of the proposed dissemination of a stabilised RF signal over a fibre loop link with passive compensation

4.1.1.   Mathematical analysis

In what follows, the steps through which the stabilised reference signal is obtained at the RS are described in detail.

It will be assumed that the MZMs have the conventional push-pull configuration, which is explained in section 3.1, and that biasing-tee elements at the electrical input connection mutually isolate the RF and biasing ports. Based on this, any continuous component in the electrical signals driving the MZMs will be discarded. Also, without loss of generality, it will be assumed that all electrical signals and optical field envelopes have a normalised amplitude.

In order to facilitate the comprehension of the analysis, the signal trip over the components of the system is divided in several steps:

1. MZM1 and OC1

At first, in the central site, the RF reference signal is generated by modulating the signal from a laser diode (LD) with an optical carrier angular frequency ω_c and optical field:

$$E_{in} = \cos(\omega_c t) \tag{4.1.1.1}$$

with a driving voltage with RF angular frequency ω_r and phase φ_r generated by a microwave source (MS):

$$V_1 = \cos(\omega_r t + \varphi_r) \tag{4.1.1.2}$$

through MZM1, which is biassed at the NP ($V_B = V_\pi$). Following the explanation of MZMs analysis in section 3.1, it is known that the MZM1 output modulated field, after been filtered in order to eliminate the non-desired harmonics, results:

$$E_1 \approx E_{in} \ \cos(\omega_r t + \varphi_r) \ = \ \cos(\omega_c t) \ \cos(\omega_r t + \varphi_r) \tag{4.1.1.3}$$

Then, without loss of generality, only the positive part of the spectrum is taken into account, and the carrier contribution is omitted in order to make the analysis centred in zero Hertzs and not in the carrier frequency f_c, resulting the optical field:

$$E_1 \approx V_1 = \cos(\omega_r t + \varphi_r) \tag{4.1.1.4}$$

with angular frequency ω_r and initial reference phase φ_r. Then, E_1 is divided into two branches (A and B) through the optical coupler (OC1) (see Figure 8 for reference).

2. PD1

The output field in branch A is detected by a photodetector (PD1) in the CS, to obtain an electrical signal as:

$$V_2' = |E_1|^2 = \cos\left(2\left(\omega_r t + \varphi_r\right)\right) + 2 \tag{4.1.1.5}$$

Then, V_2' is filtered in order to eliminate the continuous component resulted from the PD1 optical to electrical conversion, obtaining a frequency-doubled RF signal:

$$V_2 = \cos\left(2\left(\omega_r t + \varphi_r\right)\right) \tag{4.1.1.6}$$

which is going to drive MZM2. This is where the phase conjugation process will take place, but to properly understand the events, it is necessary to follow the signal over the other branch of the OC1 output.

3. SMF1, OC2 and SMF2

Going back to the end of step 1, the branch B of the OC1 injects the optical field E_1 through the fibre SMF1 towards the RS, where, affected by a noisy phase delay φ_1 when propagating through SMF1, the received field results:

$$E_2 = \cos(\omega_r t + \varphi_r - \varphi_1) \tag{4.1.1.7}$$

Then, an optical coupler (OC2) divides E_2 into branches C and D. The output field in branch C is injected through the fibre SMF2 back to the CS, where, affected by a noisy phase delay φ_2 when propagating through SMF2, the received field results:

$$E_3 = \cos(\omega_r t + \varphi_r - \varphi_1 - \varphi_2) \tag{4.1.1.8}$$

Then, the total accumulated phase change is $\varphi_s = \varphi_1 + \varphi_2$.

4. MZM2 and TOF2

Back to the end of step 2, E_3 is modulated in the MZM2 biassed at the NP ($V_B = V_\pi$, explained in section 3.1) with V_2 as the driven voltage, resulting an optical output expressed as:

$$E_4' \approx E_3 \cos(2(\omega_r t + \varphi_r)) \tag{4.1.1.9}$$

which, after include the E_3 field envelope expression and developing the cosine:

$$E_4' \approx \cos\left(3\omega_r t + 3\varphi_r - \varphi_s\right) + \cos\left(\omega_r t + \varphi_r + \varphi_s\right) \tag{4.1.1.10}$$

which contains a term at ω_r which is the phase conjugate of the optical input field E_3.

Then, filtering the relevant sidebands through the optical passband filter TOF2, the phase conjugation operation is completed and it is achieved, at the output of TOF2, an optical field:

$$E_4 = \cos\left(\omega_r t + \varphi_r + \varphi_s\right)$$

(4.1.1.11)

5. SMF2, OC2 and PD2

The field E_4 travels back to the RS through SMF2, acquiring a phase delay φ_2:

$$E_5 = \cos\left(\omega_r t + \varphi_r + \varphi_1\right)$$

(4.1.1.12)

and it is coupled through the branch E of the optical coupler OC2 to the input of the photodetector PD2, obtaining in its output, after filtering the continuous component:

$$V_3 = \cos\left(2(\omega_r t + \varphi_r + \varphi_1)\right)$$

(4.1.1.13)

6. MZM3, PD3 and EBPF

Following, the electrical signal V_3 drives the MZM3, which optical input field is (retaking step 3) E_2, retained in branch D of OC2. The MZM3 is biassed at the QP ($V_B = \frac{V_\pi}{2}$), so as explained in section 3.1, its output field results:

$$E_6 \approx E_2\left(1 + m_3 \cos\left(2\omega_r t + 2\varphi_r + 2\varphi_1\right)\right)$$

(4.1.1.14)

where m_3 corresponds to the modulation index of the MZM3. Then, substituting E_2 and developing the cosines, it is obtained:

$$E_6 \approx \cos\left(\omega_r t + \varphi_r - \varphi_1\right) + \frac{m_3}{2}\cos\left(3\omega_r t + 3\varphi_r + \varphi_1\right) + \frac{m_3}{2}\cos\left(\omega_r t + \varphi_r + 3\varphi_1\right)$$

(4.1.1.15)

As small-signal approximation is being considered (see section 3.1), $m_3 << 1$ and then the last term in equation (4.1.1.15) may be neglected:

$$E_6 \approx \cos\left(\omega_r t + \varphi_r - \varphi_1\right) + \frac{m_3}{2}\cos\left(3\omega_r t + 3\varphi_r + \varphi_1\right)$$

(4.1.1.16)

Following, the field E_6 passes through the photodetector PD3, obtaining an output electrical signal as:

$$V_4' = |E_6|^2 = \cos\left(2\omega_r t + 2\varphi_r - 2\varphi_1\right) + \frac{m_3^2}{4}\cos\left(6\omega_r t + 6\varphi_r + 2\varphi_1\right) +$$

$$+ \; m_3\cos\left(4\omega_r t + 4\varphi_r\right) + \; m_3\cos\left(2\omega_r t + 2\varphi_r + 2\varphi_1\right) + 4 \qquad (4.1.1.17)$$

Then, after passing the detected signal at the output of PD3 through an electrical bandpass filter (EPBF), the obtained electrical signal results:

$$V_4 = \cos\left(4\omega_r t + 4\varphi_r\right) \qquad (4.1.1.18)$$

which frequency and phase are four times the ones in reference RF signal V_1. Furthermore, the phase fluctuation caused by fibre links has been automatically removed.

Due to no mixers and multipliers in this scheme, undesired spurious signals are less invasive [9], and an all-optical stable quadruple frequency dissemination is easily implemented.

4.2.   Components impact to the phase compensation

Once the proposed system for the phase compensation has been theoretically analysed, it is necessary to wonder about the dissemination performance when it comes to practical experiments with real components.

In practice, MZMs do not behave exactly as anticipated in the theoretical analysis. Their cosine-shape transfer functions may lead to non-linearities in the output signals, which affects the whole system's response and therefore, the level of phase compensation achieved. For this reason, the characterization of these non-linearities will be crucial to predict the system's performance, also allowing the comparison among different realisations and devices.

The predominant sources of non-ideal behaviour in the MZMs are the extinction ratio (ER) and the modulation index m that characterise these devices:

- **The extinction ratio**

As a consequence of an non-ideal splitting ratio of the optical waveguides in the Mach Zehnder interferometer, the MZM contrast in between the maximum and the minimum values of the optical power at its output is limited.

This relation between threshold powers defines the extinction ratio (ER) of the MZM, and is defined as [23]:

$$ER = \frac{P_{max}}{P_{min}} \tag{4.2.1}$$

with P_{max} and P_{min} respectively the maximum and minimum optical power levels possibly found at the output of the MZM.

In section 3.1 an ideal case of MZM was considered, where the optical signal is equally splitted in both branches of the interferometer. Nevertheless, in practice, the input and the output of the MZM divide the power between both branches in the ratio:

$$\gamma = \frac{1-\alpha}{\alpha} \tag{4.2.2}$$

where the split ratio verifies $0 < \gamma < 1$, as can be seen in Figure 9:
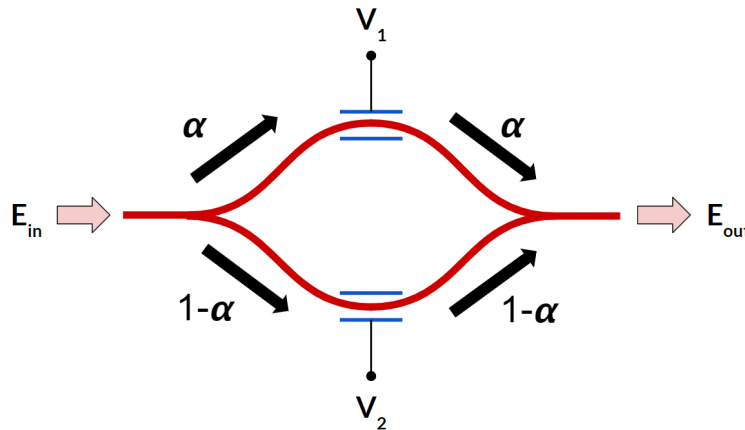
Figure 9: Asymmetric power split in MZM branches

Then, the output field in the MZM expressed in equation (3.1.3), may be written as:

$$E_{\text{out}} = E_{\text{in}} \sqrt{\alpha}\sqrt{\alpha} \, e^{j\frac{\pi V_1}{2V_\pi}} + E_{\text{in}} \sqrt{1-\alpha}\sqrt{1-\alpha} \, e^{j\frac{-\pi V_1}{2V_\pi}} \tag{4.2.3}$$

to contemplate the non-ideal asymmetric split case where $\alpha \neq \frac{1}{2}$, and so:

$$E_{\text{out}} = E_{\text{in}} \left(\alpha \, e^{j\frac{\pi V_1}{2V_\pi}} + (1-\alpha) \, e^{j\frac{-\pi V_1}{2V_\pi}} \right) \tag{4.2.4}$$

then:

$$E_{\text{out}} = E_{\text{in}} \left(e^{j\frac{\pi V_1}{2V_\pi}} + \gamma \, e^{j\frac{-\pi V_1}{2V_\pi}} \right) \qquad (4.2.5)$$

Knowing that the modulated signal maximum power level is obtained [24] at:

$$P_{max} = 1 + \gamma^2 + 2\gamma \qquad (4.2.6)$$

and, the minimum:

$$P_{min} = 1 + \gamma^2 - 2\gamma \qquad (4.2.7)$$

the influence of the splitting ratio in the ER can be expressed from equation (4.2.1) as:

$$ER = \frac{1 + \gamma^2 + 2\gamma}{1 + \gamma^2 - 2\gamma} = \left(\frac{1+\gamma}{1-\gamma} \right)^2 \qquad (4.2.8)$$

therefore, the split ratio is related with ER as follows:

$$\gamma = \frac{\sqrt{ER} - 1}{\sqrt{ER} + 1} \qquad (4.2.9)$$

where $\gamma = 1$ in the ideal case of $ER = \infty$, as the minimum power level at the output optical signal is zero.

As seen, the ER has a great impact on the MZM performance, as when the signal is not perfectly splitted, the OFF state (the minimum level of power at the output, ideally zero) contributes to base-band noise, more significant while lower ER [23].

- **The modulation index**

The modulation index of the MZM is defined as equation (3.1.10), and determines the relation between the amplitude of the RF modulating signal and the halfwave voltage.

In section 3.1 analysis, the small signal condition was assumed in an ideal situation where the modulation index of the MZM $m << 1$, supposing that the modulating signal peak power level V_{RF} was much smaller than the halfwave voltage V_π. In that case, when the MZM is operating in QP ($V_B = \frac{V_\pi}{2}$) the signal is always in the linear range of the transfer power function, as can be seen in Figure 3.

In practice, the modulation index may not be that small, leading to non-linearities at the output signal due to the driving MZM signal entering the non-linear region of the transfer function. In that case of a large m value, the influence of higher non-desired order harmonics of the RF signal due to Bessel first kind functions (see section 3.1) increases, affecting the output modulated signal.

4.3. Allan variance as a quality factor

It is a major goal to establish a quality parameter that defines the system's behaviour in relation to the frequency stability. Although several statistics can be used to calculate the amount of variation or dispersion of a set of values, the role of the Allan variance as the non-classical statistic preferred to estimate frequency stability will be discussed in this section.

On the other hand, once the Allan variance is chosen as a suitable parameter of measure for the phase instability in this system, a proper relation between its calculation parameters and the system's parameters will be crucial to obtain good and reliable results. A section of this chapter is intended to explain mathematically this relation, as well as the calculations to obtain the AVAR from the system.

4.3.1. Standard deviation and Allan deviation

When measuring frequency stability, the data set of frequency fluctuations may be characterised by flicker frequency noise, random walk noise, or other non-white-noise frequency deviation [19].

If, with the aim to calculate the frequency stability, the standard deviation is computed over the frequency fluctuations data set, it can be seen that, due to the presence of the mentioned above types of noises, the standard deviation diverges as the number of samples increases. This is, its convergence depends on the data length [25] [26].

On the other hand, the Allan deviation convergence has been verified [19] for the power law spectra mentioned above, present in oscillators. For this reason, the standard deviation is not used to characterise oscillators, and Allan variance is the indicated statistic.

4.3.2. Allan variance of the phase compensation system

In this section, the computation of the AVAR in the particular case of the phase compensation system analysed in this project is going to be explained, based on the concepts introduced in the "Previous concepts" chapter.

The estimator used for the calculation will be the overlapped variable τ estimator with equation (3.2.8), due to the better performance over the other estimators presented in the previous chapter.

First of all, the reference signal of the studied phase compensation system may be approached following the basic model of an oscillator:

$$V(t) = V_0 \sin\left(2\pi\nu_{nom}t + \varphi(t)\right) \tag{4.3.2.1}$$

where ν_{nom} is the nominal frequency in cycles per second (hertz in SI), or $\omega_{nom} = 2\pi\nu_{nom}$, the nominal angular frequency in radians per second. The total phase of the signal is composed by a perfectly cyclic component $\omega_{nom}t$ and a fluctuating component $\varphi(t)$.

If ν_{nom} is understood as the initial frequency of the signal and $\varphi(t)$ as the relative phase fluctuation in the signal propagation:

$$\varphi(t) = \varphi_{tot}(t) - \varphi_0 \tag{4.3.2.2}$$

where $\varphi_{tot}(t)$ is the total phase fluctuation of the signal, and φ_0 the initial phase of the signal.

Then, $\varphi(T)$ will be the phase compensating error, being T the amount of time it takes to the signal to propagate from the CS to the RS (in the time T, the phase has already been compensated).

If a reference signal is sent from the CS each time T and the phase is measured in the RS each T, a data set of phase-error may be formed:

$$\varphi_n = \varphi_n(T) \tag{4.3.2.3}$$

where φ_n is the phase compensating error corresponding to the nth sended reference signal, and $\varphi_n(T)$ the relative phase fluctuation of the nth sended reference signal in time T. Please note that $\varphi_n(T) \neq \varphi(nT)$, as will be clarified below.

With these measurements, a data set of fractional frequency measurements is created, and if the AVAR is computed over them, it is possible to characterise the amount of compensation achieved.

To get the fractional frequency time-series through the phase-error measurements, the frequency of the nth signal when it arrives to the RS $\nu_n(t = T)$ is computed as:

$$\nu_n(T) = \nu_n = \frac{\phi_n}{2\pi T} \tag{4.3.2.4}$$

where ϕ_n is the total phase of the signal in the instant $t = T$:

$$\phi_n = 2\pi\nu_{nom}T + \varphi_n \qquad (4.3.2.5)$$

Following, the nth fractional frequency will be calculated as indicated in (3.2.4):

$$y_n = \frac{\nu_n - \nu_{nom}}{\nu_{nom}} \qquad (4.3.2.6)$$

As can be seen, although the signals sent from CS to RS are independent one of another, the interpretation to calculate the AVAR consists of grouping them as a single oscillator whose total phase $\phi(t)$ varies from φ_0 to $2\pi\nu_{nom}T + \varphi_n$ each nT.

Then, the AVAR is computed using the overlapped variable τ estimator with equation (3.2.8), where M will be the number of measurements (i.e. number of reference signals sent from CS to RS). The observation time τ will be n times the sampling period time τ_0, which will happen to be T as the measurements are taken each T:

$$\tau_0 = T \qquad (4.3.2.7)$$

It is important to emphasise that before computing the AVAR, the average fractional frequencies $\bar{y}_n$ have to be calculated from fractional frequencies y_n, averaging them over the observation number of samples n as (3.2.2). Therefore, $\bar{y}_n$ will have $M - n + 1$ samples.

Finally, the ADEV is extracted by squaring the AVAR result, which can be plotted over $\tau = n\tau_0$ repeating the calculations over the same data set by changing the n values typically as an octave sequence as:

$$n \in \left[2^0, 2^1 \dots 2^{\left[\log_2\left(\frac{M-1}{2}\right) \right]} \right] \qquad (4.3.2.8)$$

With the ADEV plot, different noise sources (which affect the phase of the signal during the propagation and therefore the final phase-error), can be identified by observing the change in the resulting ADEV with the observation time. This is because some noise types (e.g. white phase noise) will be averaged out when the observation time increases

and therefore the ADEV will be reduced, and others will be more notable instead (e.g. random walk noise or temperature changes) [18].

5. Results

Once the system has been analysed and its theoretical results have been obtained, the practical behaviour in order to analyse the non-linearities described in section 4.2 with the Allan Variance as a metric factor is an essential part of the project.

In this chapter, a MATLAB simulation of the phase compensation system has been created with the aim to observe the level of compensation achieved with this technique, comparing cases with different levels of the components' non-linearities. Applying the calculation of the Allan variance as introduced in section 4.3.2, these cases are distinguished by this parameter, and the results compared with each other.

5.1. MATLAB simulations of the system

The MATLAB simulation is intended to reproduce the reference RF signal trip through the system described in section 4.1 steps, with fibre propagation characterised by a random phase drift.

For the simulation, the initial frequency of the RF signal is assumed to be $f_o = 1\ GHz$. Voltages and optical field envelopes as given in the theoretical analysis are represented numerically in both time and frequency domains with N = 100 samples, and the MZM transfer function considers the limiting effect of a finite ER (see sections 3.1 and 4.2). Also, for the optical filtering stages it is assumed a simple flat passband Butterworth transfer function, mathematically given by:

$$H(f) = \frac{1}{\sqrt{1 + (f/f_c)^{2n}}} \tag{5.1.1}$$

where n is the order of the filter and f_c is the cutoff frequency. For the filter at the output of MZM1, values of $n = 4$ and $f_c = 1.9\ GHz$ have been assumed, and for TOF2 $n = 8$ and $f_c = 2\ GHz$.

Then, the phase compensation error extracted from equation (4.3.2.2) is plotted for 100 reference signal trips (Figures 10-13), in which the phases acquired in SMF1 and SMF2 could randomly take any value in between 0 and 2π radians.

The simulation MATLAB code can be found in Annex 3.

5.1.1. Results in function of the modulation index

In order to see the influence of the modulation index on the phase compensation, the plots of 100 rounds are compared by changing the modulation index of the MZM3 (as is the one operating in the QP, therefore in which the m non-linearities are more significant,

see section 4.2), the Figure 10 results are obtained (in which the ER of the MZMs is assumed to be very large):
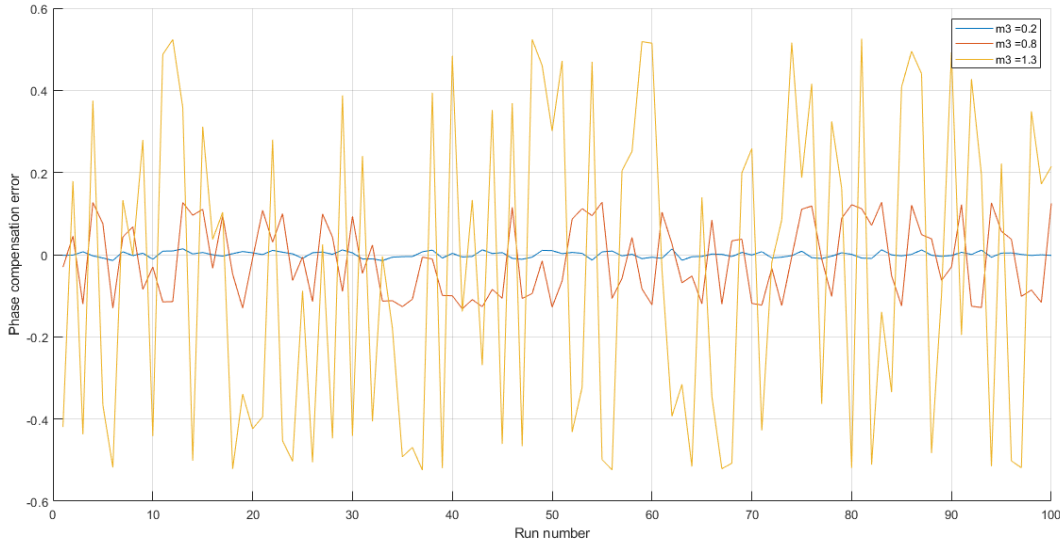

Figure 10: Phase compensation error in 100 runs of reference signal for $m_3 = 0.2$, $m_3 = 0.8$, $m_3 = 1.3$ and extinction ratio $ER = \infty$

As can be seen in Figure 10, as the modulation index increases so does the nonlinearity of the MZM. Then, the system does not behave as expected in the theoretical and ideal previously obtained results and a perfect phase compensation does not occur. Instead, an error in the compensation appears and increases as the modulation index increases, as predicted in section 4.2.

5.1.2. Results in function of extinction ratio

If the plots of 100 rounds are compared by changing the ER of the modulators, its influence to the phase compensation can be observed. The results are plotted in Figure 11, and are similar to the obtained by changing the modulation index in the previous section.

The ER simulation values are in logarithmic units, and knowing that $ER = 25\ dB$ is a common value for a MZM, it has been compared with two higher values $ER = 35\ dB$ and $ER = 40\ dB$, to see how the phase error decreases its value in the rounds as the non-linearity of the MZMs increase due to their better value of ER.
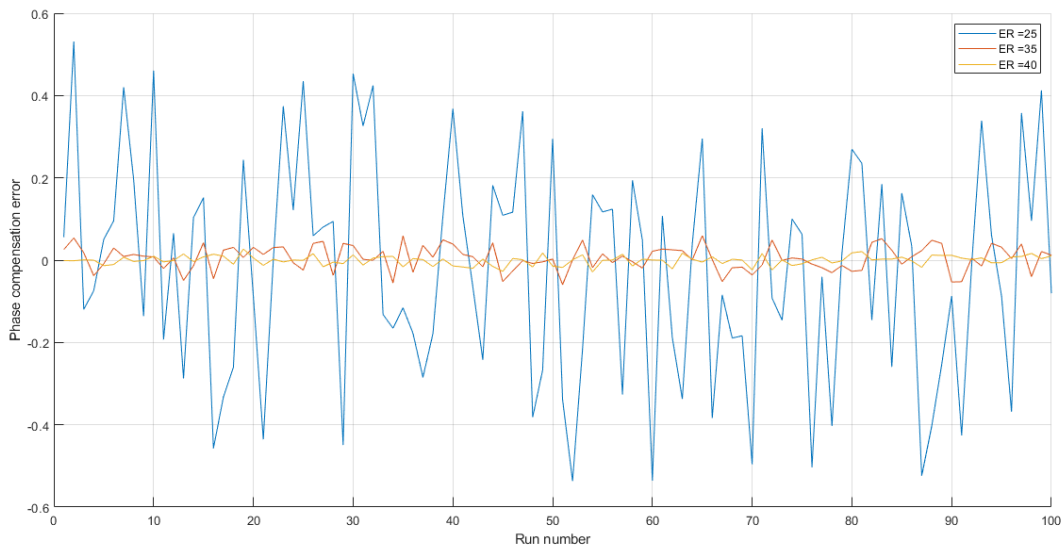
Figure 11: Phase compensation error in 100 runs of reference signal for $ER = 25 \; dB$, $ER = 35 \; dB$, $ER = 40 \; dB$ and modulating factor $m = 0.2$

5.2. Allan deviation analysis

Finally, the behaviour seen in the last section can be characterised by the Allan variance and the Allan deviation. As explained in section 3.2, these parameters will measure the frequency stability of the system, analysing the amount of change in the values of the phase compensation error.

It can be supposed by seeing Figure 10 and Figure 11 that, as more compensation is achieved, there is less difference between the phase error values in the rounds and, therefore, a better value of Allan variance will have the experiment.

To compute the AVAR and the ADEV values for the simulations, the procedure explained in section 4.3.2 is followed. Once the phase errors corresponding to 100 rounds with a certain value of m and ER are obtained, the AVAR and the ADEV are calculated over them for different observation times. In order to appreciate the effect of the observation time in the results, the acquired phases in the propagation through the fibres are still a random value between 0 and 2π radians, but now they are probably lower in the first part of the rounds and higher in the second part, simulating a change in the temperature that affects the fibre random length.

The resulting values of the ADEV in function of the observation time are plotted for the cases of m and ER in section 5.1, and then compared between them.

Furthermore, the AVAR has been also calculated with the MATLAB function *allanvar* in order to validate the results obtained in this thesis method of calculation, obtaining differences in the order of 10^(-25) between both values, which verifies the reliability of the obtained results and the interpretation of the parameter made.

5.2.1. Modulation index

The ADEV values obtained in function of the modulation index of the MZM3 and the averaging factor n (introduced in sections 3.2 and 4.3.2, as an octave sequence), are plotted in Figure 12:
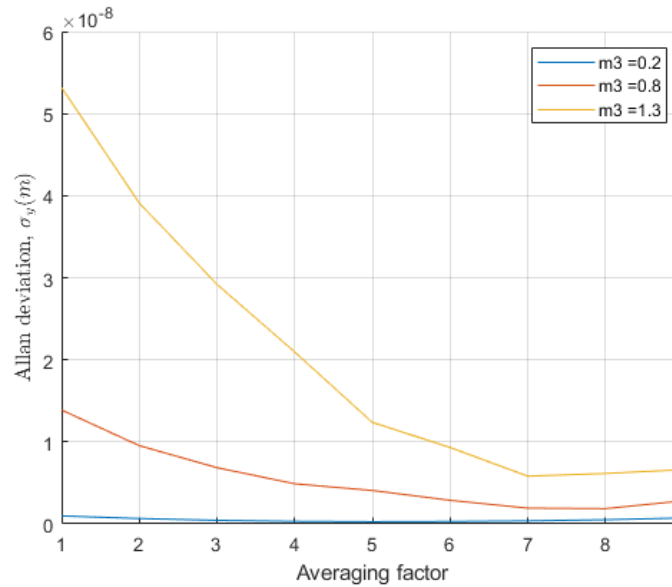

Figure 12: Allan deviation plot as a function of the averaging factor n and for $m_3 = 0.2$, $m_3 = 0.8$, $m_3 = 1.3$ and extinction ratio $ER = \infty$

As can be observed in Figure 12, the value of the ADEV improves (i.e. decreases) as the modulation index decreases, illustrating a higher frequency stability of the system as the MZM improves its performance.

It can also be seen that, at very short observation time τ, the ADEV values are higher due to the noise affecting the phase compensation. At longer observation times, the ADEV value decreases due to the noise averages out, and, at still longer τ, the ADEV starts increasing again suggesting that the temperature is affecting the fibre length and then the phase error is gradually drifting.

5.2.2. Extinction ratio

Finally, if the ADEV values are compared between the cases of ER analysed in section 5.1.2, the values shown in Figure 13 are obtained:
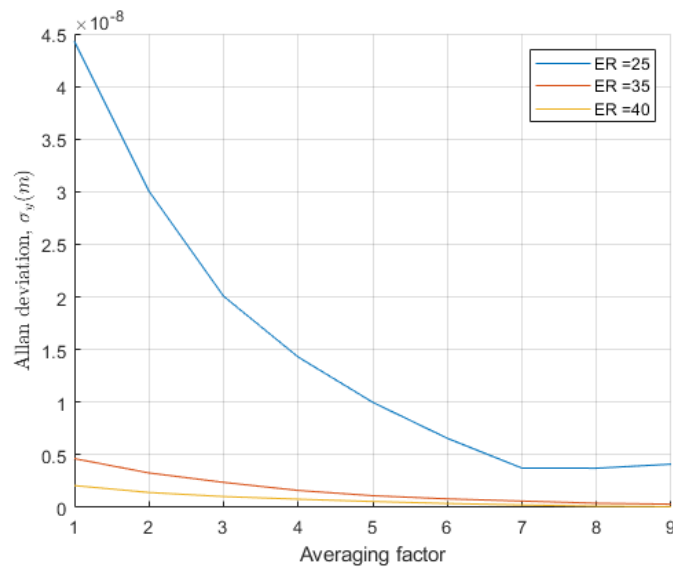
Figure 13: Allan deviation plot as a function of the averaging factor n and for $ER = 25\ dB$, $ER = 35\ dB$, $ER = 40\ dB$ and modulating factor $m = 0.2$

The results shown in Figure 13 have a similar interpretation of the ones for the modulation index. It can be seen that for smaller values of ER the ADEV results reveal a worse stability, with a great difference with higher values of ER.

6.   Budget

The development of this project has been made with no costs aside from the salary of the creators and advisors in relation to the amount of time they spent working, since the programs and equipment used have not had any additional cost.

As for myself, my salary would be similar to a junior engineer. However, my supervisor should be considered as a senior engineer and the salary goes accordingly.

	Quantity	Cost (€/h)	Time (h/week)	Nº of weeks	Total (€)
Junior engineer	1	10	22	16	3520
Senior engineer	1	20	3	16	960
				Total cost (€)	4480

Table 1: Budget analysis

The total cost of the project would be **4.480 €**

7. __Conclusions__

In this thesis, ultra-stable frequency dissemination through optical fibres has been studied, analysing a system that achieves the phase fluctuation cancellation by replacing the common electrical frequency mixing with photonic microwave phase conjugation and photomixing, thus avoiding the local oscillator leakage and mixing spurs from mixers.

The phase compensation achieved by the system has been verified both numerically and by simulations. But although the obtained results are quite impressive, an error in the phase cancellation as a consequence of the non-linearities introduced by the components integrating the system is noticed.

With the aim to characterise this phase compensation error, the practical behaviour of the components has been analysed in order to understand the possible sources of the non-linearities. Then, a method to establish a reliable performance's quality measure has been researched, to finally employ the Allan variance to measure the frequency stability of the system.

The research of the Allan variance concept and calculation has led to the possibility of characterising the system. Through simulations, the well understanding of the parameter has been proven, and the influence of the components' non-linearities in the system's performance has been measured.

Bibliography

[1] D. Marpaung, J. Yao and J. Capmany. *Integrated Microwave Photonics*. Nature Photonics vol. 13, 2019.

[2] H. Wang, S. Li, X. Xue, X. Xiao and X. Zheng. *Distributed Coherent microwave photonic radar with a high precision fiber-optic time and frequency network*. Optics Express vol. 21, no. 21, 2020.

[3] J. Dong, F. Zhang, Z. Jiao, Q. Sun and W. Li. *Microwave photonic radar with a fiber-distributed antenna array for three-dimensional imaging*. Optics Express vol. 28, no. 13, 2020.

[4] H. Si, B. Wang, F. Wang, Y. Chen and L. Wang, *Absolute phase synchronization over optical fiber*. Optics Express vol. 28, no. 4, 2020.

[5] S. Pan, J. Wei and F. Zhang. *Passive phase correction for stable radio frequency transfer via optical fiber*. Photon. Netw. Commun, vol. 31, 2016.

[6] Y. He. *Long-distance telecom-fiber transfer of a radio-frequency reference for radio astronomy*. Optica vol. 5, no. 2, 2018.

[7] W. Li, W. T. Wang, W. H. Sun, W. Y. Wang, N. H. Zhu. *Stable radio-frequency phase distribution over optical fiber by phase-drift autocancellation.* Optics Letters vol. 39, no. 5, 2014.

[8] F. Yin, A. Zhang, Y. Dai, T. Ren, K. Xu, J. Li, J. Lin and G. Tang. *Phase-conjugation-based fast RF phase stabilization for fiber delivery*. Optics Express vol. 22, no. 1, 2014.

[9] H. Wang, X. Xue, S. Li and X. Zheng. *All-optical Arbitrary-Point Stable Quadruple Frequency Dissemination with Photonic Microwave Phase Conjugation.* IEEE Phot. Journal vol. 10, no. 4, 2018.

[10] Y. Li, Y. Zhang, Y. Huang. *Any bias point control technique for Mach-Zehnder Modulator*. IEEE photonics technology letters, vol 25, No. 24, December 2013, p 2412-2415.

[11] Hongxian Chen, et al., *Nonlinear distortion evaluation of MZM with equivalent mathematical model calculation in IM/DD OOFDM transmission system*. Changsha, China, November 2013.

[12] D. Chatterjee. *A theoretical investigation of fiber phase sensitive amplifiers for applications*. Paris, France, January 2021.

[13] D. Rörich, X. Wang, M. Bernhard, J. Speidel. *Optimal Modulation Index of the Mach-Zehnder Modulator in a Coherent Optical OFDM System Employing Digital Predistortion*. Stuttgart, Germany, 2013.

[14] M. Abramowitz, I. Stegun. *Handbook of Mathematical Functions with Formulas, Graphs, and Mathematical Tables*. USA, June 1964.

[15] *Bessel Functions of the First and Second Kind*. (PDF). *mhtlab.uwaterloo.ca*. p. 3. Retrieved 24 May 2022.

[16] Derek Y. Kubo, et al., *Development of a Mach-Zehnder Modulator Photonic Local Oscillator Source.* IEEE, August 2013.

[17] *Bessel Functions.* (PDF) sharif.edu. Retrieved 30 May 2022.

[18] David W. Allan. *Time and Frequency (The-Domain) Characterization, Estimation, and Prediction of Precision Clocks and Oscillators*. IEEE, November 1987.

[19] James A. Barnes, et al., *Characterization of Frequency Stability*. IEEE, May 1971.

[20] D. A. Howe, D. W. Allan, and J. A. Barnes. *Properties of Signal Sources and Measurement Methods*. Colorado, USA, 1981.

[21] J. J. Snyder. *An ultra-high resolution frequency meter*. pages 464–469, Frequency Control Symposium #35, 1981.

[22] *Definitions of physical quantities for fundamental frequency and time metrology – Random Instabilities*. IEEE STD 1139-1999. 1999.

[23] Ivan P. Kaminow and Thomas L. Koch. *Optical Fiber Telecommunications IIIB*, 3rd ed. New Jersey, Academic Press, 1997.

[24] J. Díaz. *Métodos de caracterización de moduladores electro-ópticos.* M.S. thesis, Escola d'Enginyeria de Telecomunicació i Aeroespacial de Castelldefels, Universitat Politècnica de Catalunya, Barcelona, 2011.

[25] D. W. Allan. *Statistics of atomic frequency standards*. IEEE, 1966.

[26] J. A. Barnes*. Atomic timekeeping and the statistics of precision signal generators.* IEEE, 1966.

Appendices

Appendix 1: MATLAB code made to represent the field and power transfer functions of a Mach-Zehnder modulator in push-pull configuration, with operation point for quadrature point (QP) and for null point (NP).

Appendix 2: Plot of Bessel functions of the first kind, for orders 0, 1 and 2.

Appendix 3: MATLAB code made to the system simulations and AVAR and ADEV calculation. Function to calculate the AVAR.

Glossary

- **RF**: Radio frequency
- **MZM**: Mach-Zehnder modulator
- **ER**: Extinction ratio
- **ADEV**: Allan deviation
- **AVAR**: Allan variance
- **CS**: Central site
- **RS**: Remote site
- **QP**: Quadrature point
- **NP**: Null point